

Dielectric and piezoelectric properties of percolative three-phase piezoelectric polymer composites

Udhay Sundar, Kimberly Ann Cook-Chennault, Sankha Banerjee, and Eric Refour

Citation: *Journal of Vacuum Science & Technology B* **34**, 041232 (2016); doi: 10.1116/1.4955315

View online: <https://doi.org/10.1116/1.4955315>

View Table of Contents: <http://avs.scitation.org/toc/jvb/34/4>

Published by the [American Vacuum Society](#)

Articles you may be interested in

[Energy harvesting from low frequency applications using piezoelectric materials](#)

Applied Physics Reviews **1**, 041301 (2014); 10.1063/1.4900845

[Study of dielectric and piezoelectric properties of CNT reinforced PZT-PVA 0-3 composite](#)

AIP Conference Proceedings **1728**, 020341 (2016); 10.1063/1.4946392

[Piezoelectricity of a high-content lead zirconate titanate/polymer composite](#)

Journal of Applied Physics **53**, 4328 (1982); 10.1063/1.331211

[Ferroelectric polymer-ceramic composite thick films for energy storage applications](#)

AIP Advances **4**, 087117 (2014); 10.1063/1.4892961

[Study of piezoelectric filler on the properties of PZT-PVDF composites](#)

AIP Conference Proceedings **1916**, 030006 (2017); 10.1063/1.5017439

[Dielectric and energy storage performances of PVDF-based composites with colossal permittivity Nd-doped BaTiO₃ nanoparticles as the filler](#)

AIP Advances **7**, 125104 (2017); 10.1063/1.5003292



Instruments for Advanced Science

Contact Hiden Analytical for further details:
W www.HidenAnalytical.com
E info@hiden.co.uk

CLICK TO VIEW our product catalogue




Gas Analysis

- dynamic measurement of reaction gas streams
- catalysis and thermal analysis
- molecular beam studies
- dissolved species probes
- fermentation, environmental and ecological studies



Surface Science

- UHV-TPD
- SIMS
- end point detection in ion beam etch
- elemental imaging - surface mapping



Plasma Diagnostics

- plasma source characterization
- etch and deposition process reaction kinetic studies
- analysis of neutral and radical species



Vacuum Analysis

- partial pressure measurement and control of process gases
- reactive sputter process control
- vacuum diagnostics
- vacuum coating process monitoring

Dielectric and piezoelectric properties of percolative three-phase piezoelectric polymer composites

Udhay Sundar and Kimberly Ann Cook-Chennault^{a)}

*Mechanical and Aerospace Engineering Department, Rutgers, the State University of New Jersey,
98 Brett Road, Piscataway, New Jersey 08854-8058*

Sankha Banerjee

*Department of Mechanical Engineering, California State University, Fresno, 2320 E San Ramon Ave.,
Fresno, California 93740*

Eric Refour

*Electrical and Computer Engineering, Virginia Polytechnic Institute and State University,
1185 Perry Street, Blacksburg, Virginia 24061*

(Received 24 December 2015; accepted 17 June 2016; published 27 July 2016)

Three-phase piezoelectric bulk composites were fabricated using a mix and cast method. The composites were comprised of lead zirconate titanate (PZT), aluminum (Al), and an epoxy matrix. The volume fraction of the PZT and Al was varied from 0.1 to 0.3 and 0.0 to 0.17, respectively. The influences of an electrically conductive filler (Al), polarization process (contact and Corona), and Al surface treatment, on piezoelectric and dielectric properties, were observed. The piezoelectric strain coefficient, d_{33} , effective dielectric constant, ϵ_r , capacitance, C , and resistivity were measured and compared according to polarization process, the volume fraction of constituent phases, and Al surface treatment. The maximum values of d_{33} were ~ 3.475 and ~ 1.0 pC/N for corona and contact poled samples, respectively, for samples with volume fractions of 0.40 and 0.13 of PZT and Al (surface treated), respectively. Also, the maximum dielectric constant for the surface treated Al samples was ~ 411 for volume fractions of 0.40 and 0.13 for PZT and Al, respectively. The percolation threshold was observed to occur at an aluminum volume fraction of 0.13. The composites achieved a percolated state for Al volume fractions >0.13 for both contact and corona poled samples. In addition, a comparative time study was conducted to examine the influence of surface treatment processing time of aluminum particles. The effectiveness of the surface treatment, sample morphology and composition was observed with the aid of scanning electron microscope and energy dispersive x-ray spectroscopy images. These images were correlated with piezoelectric and dielectric properties. © 2016 American Vacuum Society.

[<http://dx.doi.org/10.1116/1.4955315>]

I. INTRODUCTION

Two-phase piezoelectric composites, comprised of piezoelectric particles embedded within a continuous polymer matrix, have attracted much attention due to their flexibility and ease of processing,^{1,2} and applications to dielectric,^{3–5} sensing/actuating,^{6–9} energy harvesting,^{1,9,10} and acoustic damping^{11–13} applications. However, these materials suffer from relatively small values of piezoelectric and dielectric properties due to the inherent insulative properties of the polymer matrix phase,^{14–18} which is associated with difficulties in the polarization of these materials¹⁹ and contact resistance at the particle/matrix interface.^{3,5} Hence, researchers have begun to investigate three-phase materials comprised of piezoelectric and electrically conductive particles embedded in a continuous polymer matrix.²⁰ In some cases, these three-phase composites have demonstrated enhanced dielectric, piezoelectric, and acoustic dampening when close to the percolation threshold.^{21,22}

In this work, the influences of three entities on the piezoelectric and dielectric properties are observed: volume

fractions of constituent phases [lead zirconate titanate (PZT) and Al], polarization technique (contact and contactless—corona), and surface treatment of the electrically conductive phase, Al. The volume fractions of PZT and Al were varied from 0.1 to 0.3 and 0.01 to 0.17, respectively. Composites were independently parallel-plate contact or corona poled. Also, composites that included nonsurface treated Al particles were compared to those that included surface treated Al particles. A detailed time study was conducted to elucidate the optimal time for surface treatment of the Al particles. The piezoelectric strain coefficients and effective dielectric constants were observed to identify the percolation threshold of the Al particles within the piezoelectric polymer composites.

Many researchers have studied the influence of conductive fillers on 0–3 composite materials and the formation of percolated networks of these fillers. However, less is known about the role that the polarization technique (contact and corona) plays on the piezoelectric and dielectric properties of three-phase materials. For example, several researchers have studied the influence of electrically conductive inclusions on piezodamping and related it to the electrically conductive network (percolation) formed by the inclusions.

^{a)} Author to whom correspondence should be addressed; electronic mail: kacook@jove.rutgers.edu

TABLE I. Overview of the data sets prepared for the time study of the aluminum surface treatment and polarization studies. Control 1 is the aluminum powder that was subjected to no ethanol treatment. Control 1 is compared to aluminum powders that were surface treated with ethanol (data sets A–F) for 0.25, 0.5, 1, 2, 3 and 4 h, respectively. Control 2 is the three-phase composite that was fabricated with aluminum that was not surface treated and parallel-plate contact polarized. Data sets G, H and I are compared to control 2.

Data set Composition (description)	Poling technique	Surface treatment of aluminum	Volume fractions A minimum of three samples prepared for each volume fraction
Control 1 Aluminum powder only	n/a	0 h	n/a
A, B, C, D, E, F Aluminum powder only	n/a	0.25, 0.5, 1, 2, 3 and 4	n/a
Control 2 PZT-epoxy-Al composite	Contact poled	None	v_{PZT} : 0.20–0.40 v_{Al} : 0.0–0.17
G PZT-epoxy composite	Corona poled	None	v_{PZT} : 0.20–0.60 v_{Al} : 0.0
H PZT-epoxy-Al composite	Corona poled	None	v_{PZT} : 0.20–0.40 v_{Al} : 0.0–0.17
I PZT-epoxy-Al composite	Corona poled	Ethanol treatment of aluminum for 4 h	v_{PZT} : 0.20 – 0.40 v_{Al} : 0.0 to 0.17

Zhang *et al.* and Ding and Yan^{23,24} fabricated two-phase chlorinated polyethylene (CPE) barium titanate and CPE and 2'-methylene-bis-(4-methyl-6-cyclohexylphenol) composites and compared the piezodamping of these materials to those where electrically conductive vapor-grown carbon fibers were added. It was concluded that the piezodamping effect was directly related to the electrically conductive network formed by the carbon fibers within the polymer matrix. It was found that this network contributed to increased loss factors, $\tan\delta$, and more efficient damping.²⁵ Choi *et al.*²¹ prepared composites, which were comprised of barium titanate, polymethyl methacrylate, and nickel using a two-step mixing and hot-molding process. It was found that the size of the nickel particles played a role in the dielectric constant, wherein composites that contained smaller sized nickel particles (4 μm) had higher dielectric constants and dielectric loss near the percolation threshold, in comparison to composites that contained larger sized particles (40 μm). Similarly, Banerjee *et al.* explored the dielectric properties of two-phase composites that incorporated a third electrically conductive phase (aluminum^{3–5,7} and multiwalled carbon nanotubes²⁶). It was found that the inclusion of electrically conductive particles within a two-phase piezoelectric composite (PZT and epoxy) resulted in enhanced piezoelectric and dielectric properties, with corresponding increases in dielectric loss of the material. Also, it was concluded that the electrically conductive filler size, distribution, and particle–matrix resistance play key roles in the dielectric and piezoelectric properties of the composites. It is well known that aluminum when exposed to air forms an Al_2O_3 shell around the Al core. As a result, the aluminum particle immediately develops positive charges in the core and negative charges around the shell due to charge transfer from aluminum to absorbed O_2 ,²⁷ which affects the properties of the interface between the aluminum and the epoxy matrix and consequently the piezoelectric and dielectric properties of the composite.

In this work, a time study of the surface treatment of Al particles was conducted to understand the role of the particle/matrix interfacial properties on composite piezoelectric and dielectric properties. Also, the piezoelectric and dielectric properties of bulk PZT-Al-epoxy composites are observed as functions of frequency, composition, and polarization method.

II. EXPERIMENTAL SETUP AND METHODOLOGY

PZT-Al-epoxy composites were fabricated where the volume fractions of PZT and Al were varied from 0.20 to 0.40 and 0.0 to 0.17, respectively. An overview of the samples and polarization techniques used is provided in Table I. The control samples and powders were prepared as described in Figs. 1 and 2. A minimum of six samples was prepared for each volume fraction and polarization scenario analyzed.

A. Materials

The materials used in all experiments were PZT-855 (Navy Type VI)²⁸ powder (APC International), DGEBA, Epofix TM Cold-setting embedding resin (electron microscopy sciences), and aluminum—99.97%, 200 mesh, i.e., $\sim 75 \mu\text{m}$ (Acros Organics). An additional set of composites that incorporated nanosized aluminum powder (instead of micron-sized aluminum powder) was fabricated, where the aluminum was 99.95% purity with spherical morphology (APS: 18 nm) and purchased from MTI. Homogenous samples of the epoxy and PZT were prepared to obtain the electrical and physical properties presented in Table II, while the Al properties were obtained from the manufacturer.

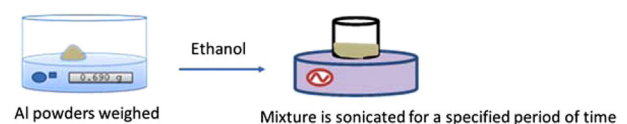


Fig. 1. (Color online) Al powder data sets A–F were sonicated in 15 ml of ethanol for 0.25, 0.5, 1, 2, 3, and 4 h. The size, morphology, and distribution (agglomeration) of the particles were observed with the aid of SEM and EDS.

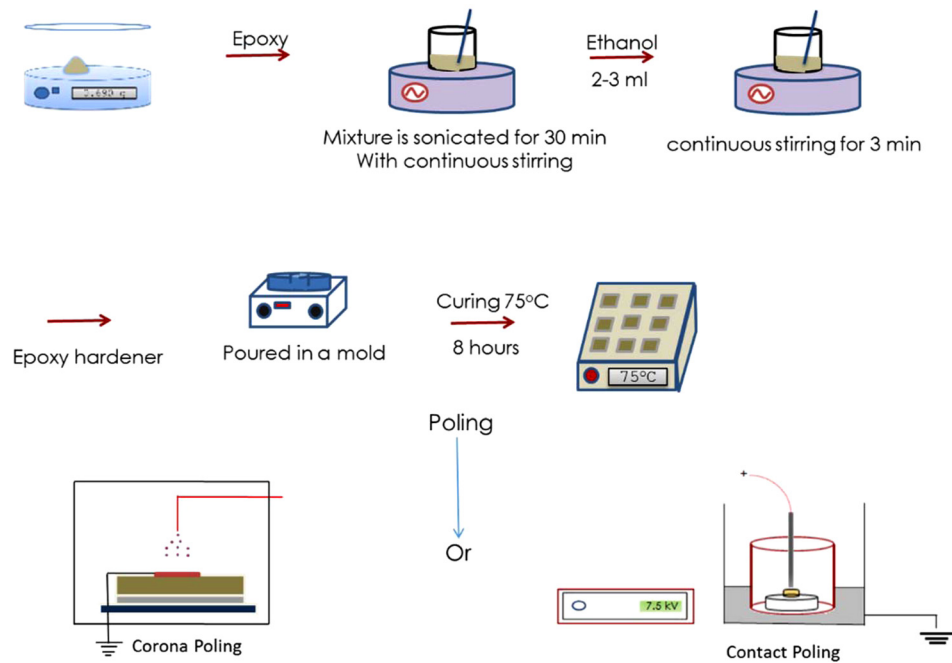


FIG. 2. (Color online) PZT and Al powders are weighed and processed accordingly. The powder mixture was then combined with epoxy, mixed by hand, and sonicated for 30 min. The mixture was then combined with ethanol, stirred, and then poured into a mold. Once in the mold, the mixture was cured in air for 8 h at 75 °C. Subsequent samples were either contact or corona poled.

B. Surface treatment of aluminum: A time study

The bond strength between the embedded particles and polymer matrix plays a critical role in the interfacial properties and resulting macroscopic properties of the composite. Also, the processing of the aluminum influences the composition of the outer shell of the aluminum. Hence, a time study of the surface treatment of the aluminum with ethanol was conducted. An overview of this processing technique is depicted in Fig. 1. In this process, Al powder was weighed and placed in a beaker with 15 ml of ethanol. A paraffin film was placed at the top of the beaker to prevent evaporation of the ethanol into the air. Several mixtures (data sets: A–F, described in Table I) were prepared and sonicated for 0.25, 0.5, 1, 2, 3, and 4 h, respectively. Once the optimal surface treatment time was observed for the micron-sized aluminum particles, this surface treatment time was used on the nanosized aluminum particles prior to the fabrication of the nanocomposites. The particle size, morphology, and distribution of the Al particles were observed with the aid of a Zeiss Sigma field

emission scanning electron microscope (SEM) and an Oxford INCA PentaFETx3 8100 energy dispersive x-ray spectroscopy (EDS). The surface treatment that minimized the agglomeration of the Al powder was selected for use in fabrication of composites observed for data set I (described in Table I).

C. Composite preparation

An overview of the fabrication process for the three-phase composites is provided in Fig. 2. First, the PZT, Al, and epoxy were weighed to achieve the desired volume fraction and combined. The Al was surface treated with ethanol for 4 h for data set I (described in Table I) prior to mixing with the PZT and Al. The mixture was subsequently hand stirred and sonicated in an ultrasonicator for 30 min. Ethanol was then added to the mixture, which was then sonicated for an additional 30 min. The epoxy hardener was then added to the mixture. The final compound was poured into a mold and cured in air for 8 h at 75 °C. The surfaces of the samples were then polished and coated with colloidal silver solution. The volume fractions of

TABLE II. Physical, dielectric and piezoelectric properties of the PZT, epoxy and aluminum (Al).

Property	PZT 855	Epoxy	Al
Relative dielectric constant, ϵ_r	3300	2.9–3.7	1.6–1.8
Dielectric dissipation, $\tan \delta$	≤ 2.50	~ 0.02 –0.04	—
Electromechanical coupling, k_p/k_{33}	0.68/0.76	—	—
Piezoelectric charge constant, d_{33} (10^{-12} C/N)	630 ^a	12.28 ^a	1.6–1.8
Young’s modulus, Y_{11}^E/Y_{33}^E (10^{10} N/m ²)	5.9/5.1	0.15–0.20	6.89
Density (g/cm ³)	7.6	(In the wet-state) 1.16 g/cm ³	2.7
Electrical resistivity (Ω cm)	49.27 ^a at 1 kHz	0.15 at 1 kHz	3.99×10^{-6}

^aExperimental values.

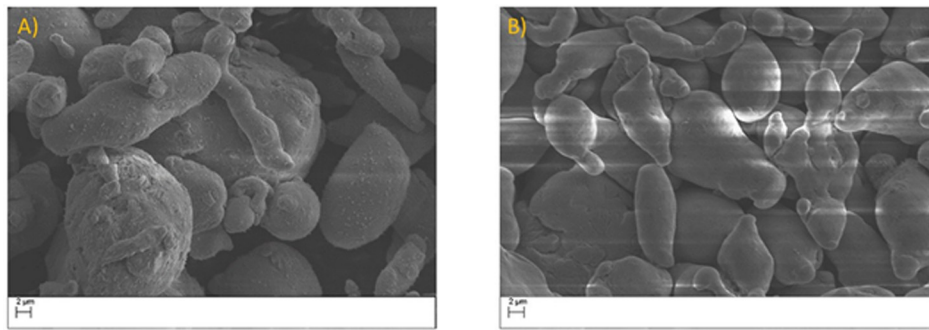


FIG. 3. (Color online) SEM micrograph images of aluminum powder that was (a) not surface treated with ethanol ($5.15\times$ magnification). The average aluminum particle size is $\sim 13.43\ \mu\text{m}$, and (b) ultrasonicated with the solvent, ethanol, for 4 h ($5.21\times$ magnification), where the average particle size was observed to $\sim 5.05\ \mu\text{m}$.

PZT and Al were varied from 0.20 to 0.40 and 0.0 to 0.17, respectively. A minimum of six samples was prepared for each volume fraction examined. All samples were polarized at 12–15 kV/cm at 65°C for 15 min. The samples prepared for control 2 were contact poled, and the samples prepared for data sets G, H, and I were corona poled. The duration of electrical polarization was held constant for both contact and corona poling; however, the contact poling was performed in a silicon bath to ensure uniform heating of the sample.

D. Dielectric and piezoelectric characterization

The longitudinal piezoelectric strain coefficient, d_{33} , and capacitance, C , were measured using a Piezo Meter System manufactured by Piezo Test, Piezoelectric Materials & Device Testing Company while the resistance was obtained using an Impedance/Gain-Phase Analyzer (HP4194A).

The dielectric constant was calculated using the expression

$$\varepsilon_r = \frac{Ct}{A\varepsilon_0}. \quad (1)$$

In Eq. (1), C is the capacitance in Farads, A is the area of the sample, ε_0 is the permittivity of free space ($\approx 8.854 \times 10^{-12}\ \text{F m}^{-1}$), and t is the thickness of the sample. The impedance analyzer was used to measure the real part of the resistance, R , of each sample, and the resistivity was determined from Eq. (2)

$$\rho = \frac{RA}{t}. \quad (2)$$

III. RESULTS AND DISCUSSION

Aluminum powder was surface treated with ethanol for time periods of 0.25, 0.5, 1, 2, 3, and 4 h to determine the appropriate sonication time required for minimal agglomeration of the aluminum particles. PZT-epoxy composites were fabricated using the corona poling technique for data set G. PZT-Al-epoxy composites were fabricated using Al powder that was not surface treated and contact (control 2) or corona poled (data set H). PZT-Al-epoxy composites were fabricated using Al powder that was surface treated for 4 h (data set I). The volume fractions of PZT and Al were varied from 0.2 to 0.4 and 0 to 0.17, respectively. The longitudinal piezoelectric strain coefficient, d_{33} was measured at 110 Hz while the dielectric constant, ε_r , and resistance were measured as a function of frequency.

A. Surface treatment of aluminum: A time study and surface morphological characterization

The size, shape, surface morphology, and degree of agglomeration of the aluminum powder were observed using a SEM and EDS. SEM images were coupled with software packages, IMAGEJ and PHOTOSHOP CS5.1, to ascertain the

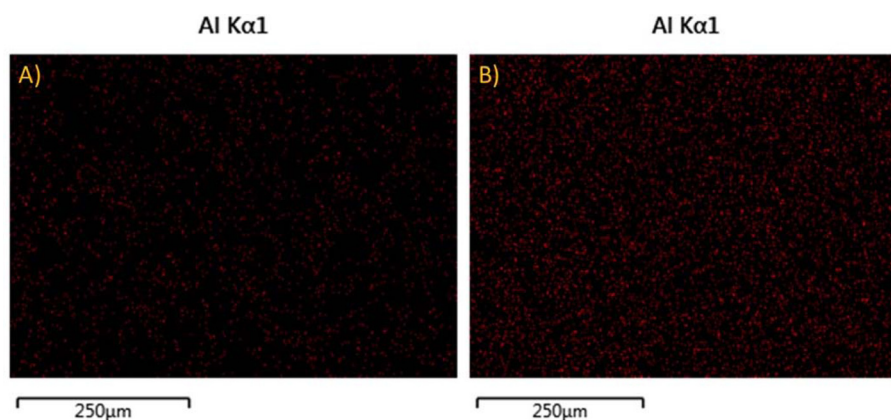


FIG. 4. (Color online) EDS micrograph images of aluminum powder that was (a) not surface treated with ethanol and (b) surface treated with ethanol for 4 h. The images indicate that the surface treated Al powder was more distributed across the matrix, in comparison to the Al powder that was not surface treated.

average particle size. The aluminum powder was surface treated with ethanol using an ultrasonicator for time periods of 0.25, 0.5, 1, 2, 3, and 4 h to determine the sonication time that would render the minimal degree of agglomeration and most consistent particle size of the aluminum. In Figs. 3 and 4, SEM and EDS micrographs are presented for Al powder that was surface treated with ethanol for 0.0 and 4 h, respectively. The average size of the nontreated aluminum was $\sim 13.43 \mu\text{m}$ while the average size of the aluminum that was ultrasonicated with ethanol for 4 h was $5.05 \mu\text{m}$. The SEM images indicate that the exposure of the aluminum to ethanol over extended periods of time diminished the agglomeration of the aluminum particles and reduced the size of the aluminum particle, as seen in Fig. 3. The surface treatment of the micron-sized aluminum particles and particle bundles for 4 h in ethanol reduced the oxide layer thickness of the Al_2O_3 layer that covered the aluminum particles and agglomerated particles. In theory, this was achieved when the ethanol chemically reacted with the Al_2O_3 shell to form ethane, where oxygen molecules in Al_2O_3 combined with hydrogen molecules of ethanol, thereby reducing the oxide layer around the aluminum particle.^{29,30} The Al_2O_3 oxide layer is subsequently destabilized from the chemical reaction between it and the ethanol. The formation of ethylene from the dehydration of ethanol³¹ could render the outer surface of the oxide layer charged. The formation of ethylene contributes to the separation of aluminum particles and subsequent repulsion force between aluminum particles that leads to the observed deagglomeration. The smaller particles that have charged surfaces separate easily and distribute more readily within the matrix, thereby improving particle distribution within the matrix as observed in the EDS images in Fig. 4. While localized aggregation may still exist, the distribution of Al has been enhanced, leading to fairly consistent values.

B. Piezoelectric and dielectric characterization

In Fig. 5, the piezoelectric strain coefficients of the two-phase composites, data set G, (corona polarized at 15 kV/cm) are plotted as a function of PZT volume fraction (from 0.2 to

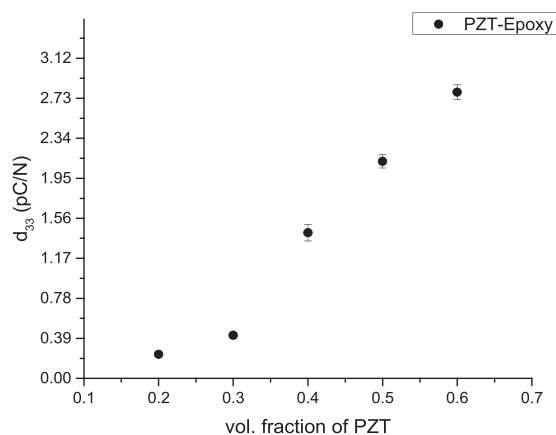


FIG. 5. Piezoelectric strain coefficient, d_{33} , for the PZT-epoxy composites (data set G) that were corona poled at 15 kV/cm are plotted as a function of PZT volume fraction. The maximum d_{33} value occurs 2.73 pC/N at a PZT volume fraction equal to 0.6.

0.6). As expected, the piezoelectric strain coefficient increases with the volume fraction of PZT content. The piezoelectric strain coefficients for control 2, data set H and data set I are plotted as a function of aluminum volume fraction, for PZT volume fractions of 0.2, 0.3, and 0.4, in Fig. 6. Control 2 was contact polarized at 12 kV/cm using nonsurface treated aluminum. Data set H was corona polarized at 15 kV/cm using nonsurface treated aluminum. Data set I was corona polarized at 15 kV/cm using aluminum that was surface treated in ethanol for 4 h. The piezoelectric strain coefficients increase with PZT and aluminum content up to an aluminum volume fraction of 0.13, beyond which there is a sharp decline in d_{33} values. This increase in d_{33} values is consistent with the observations of Refs. 14, 17, and 32–35, which measured increases in d_{33} as PZT content increased within piezoelectric polymer composite. The particle size and relative density of the composites influence the effective piezoelectric strain and dielectric constants of the piezoelectric composite materials.

In this work, the d_{33} values are relatively small in comparison to some values reported by others (Table I). The differences in the piezoelectric strain values are most likely due to the use of small size and volume fraction of PZT particles, which were $\sim 3 \mu\text{m}$ and 0.40 volume fraction (in this work) and differences in the matrix materials used for this work and the work of the others. For example, Nhuapeng and Tunkasiri³² and Rujijanagul *et al.*^{36,37} used piezoelectric particles sizes that were ~ 160 and $875 \mu\text{m}$, respectively, with PZT volume fractions that were greater than 0.50. These results agree with the conclusions of Rujijanagul *et al.* and Banerjee *et al.*,^{3,5,36} who concluded that two-phase

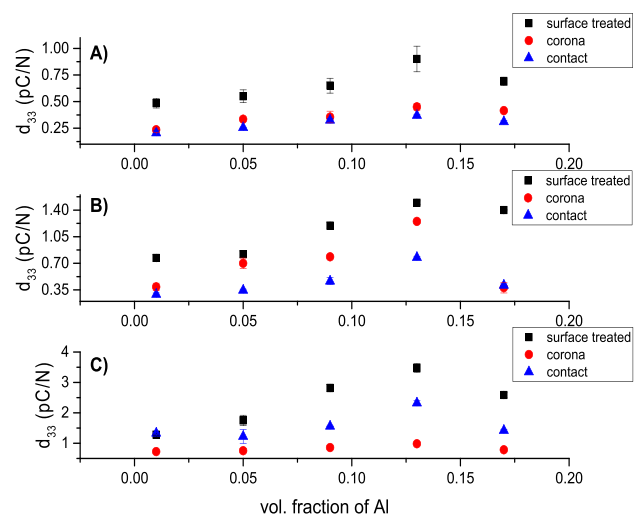


FIG. 6. (Color online) Piezoelectric strain coefficient, d_{33} , for control 2 (contact poled at 12 kV/cm and nonsurface treated Al), data set H (corona poled at 15 kV/cm and nonsurface treated Al) and data set I (corona poled at 15 kV/cm and surface treated Al for 4 h) as a function of aluminum volume fraction for a constant PZT volume fraction equal to 0.02, 0.03, and 0.04. The maximum d_{33} values occur when the volume fraction of aluminum is equal to 0.13 for all volume fractions of PZT. The volume fraction of PZT is held at (a) 0.02 where the maximum d_{33} values are 0.37, 0.45, and 0.9 pC/N for control 2, data set H and data set I, respectively; (b) 0.03 where the maximum d_{33} values are 0.78, 1.25, and 1.50 pC/N for control 2, data set H and data set I, respectively; and (c) 0.04 where the maximum d_{33} values are 0.99, 2.32, and 3.48 pC/N for control 2, data set H and data set I, respectively.

piezoelectric composites that incorporate ceramic powder particles with larger particle sizes lead to higher effective piezoelectric strain coefficients than composites with smaller size piezoelectric particles. Rujijanagul *et al.* also stated that these higher values were mostly because larger sized piezoelectric particles have a higher surface energy than smaller powder particle sizes, which was because the contact surface area between the bigger ceramic powder particles and the polymer was larger than that of smaller ceramic particles. Hence, Rujijanagul *et al.*³⁶ concluded that larger size powder particles achieve more effective polarization in the composite than smaller powder particles in a polymer matrix. Also, many of the other composites listed in Table III included matrix materials that were piezoelectric, such as polyvinylidene fluoride, or polyvinylidene difluoride (PVDF). Since the matrix material was piezoelectric (PVDF), the effective piezoelectric properties of the composites were greater in value than the ones described herein. The range of d_{33} depicted in Fig. 5 is consistent with the work of Ref. 36 where the average particle size was less than $34\text{ }\mu\text{m}$ (poling voltage at 10 kV/cm and room temperature), which is consistent with the polarization voltages used in this work.

The two-phase piezoelectric composites with PZT volume fractions of 0.2 and 0.3 that were Corona polarized had d_{33} values that were greater than those measured for three-phase composites from data set G that were contact polarized. On the other hand, at the PZT volume fraction that was equal to 0.4, the corona polarized two-phase composite (data set G) was higher than control 2 (PZT volume fraction equal to 0.4). The contribution of the aluminum inclusions are not clearly observed at higher PZT volume fractions in contact poled samples, as shown in Fig. 6(a). This observation is most likely due to problems associated with the difficulty of achieving the desired polarization voltage of $\sim 12\text{ kV/cm}$ in

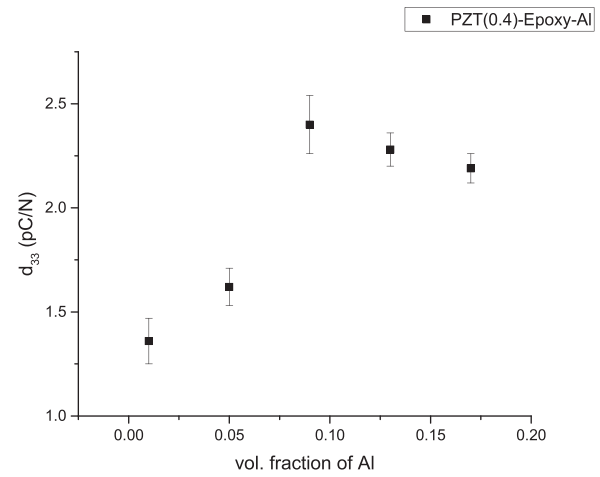


FIG. 7. Piezoelectric strain coefficient, d_{33} , is plotted as a function of nano-sized aluminum volume fraction for a constant volume fraction of 0.40 for PZT. The samples were corona poled at 15 kV/cm and surface treated nano-sized aluminum for 4 h. The maximum d_{33} value is 2.4 pC/N for 0.40 and 0.09 volume fractions of PZT and aluminum, respectively.

the parallel-plate contact polarized samples. The composites that were corona polarized (data sets H and I) benefited from the aluminum inclusions, as opposed to those composites that were contact polarized. In corona poling, charged ions adhere to the surface of an electrode sample, thereby creating an electric potential between the sample's top surface and the grounded plate.¹⁹ Thus, samples with defects and electrically conductive inclusions can be polarized at higher voltages using the corona poling process. In both the corona and contact poled samples, d_{33} ceased to increase beyond an aluminum volume fraction of 0.13, which is most likely due to the electrical percolation of the aluminum. The percolation volume fraction is smaller than the theoretical prediction range: 0.15–0.17,³⁸ which is valid for

TABLE III. Dielectric and piezoelectric properties of the PZT polymer composites and comparison with those of previous workers (Refs. 32 and 44–49).

Sample	Volume fraction % PZT/epoxy/Al	Dielectric constant, ϵ_r	d_{33} (pC/N)
PZT/DEGBA epoxy/Al (control 2, this work)	40/47/13	~ 270	0.99
PZT/DEGBA epoxy (data set G, this work)	40/60/0	~ 134	1.36
Control 2, PZT/DEGBA epoxy/Al (data set H, this work)	40/47/13	~ 305	2.32
PZT/DEGBA epoxy/Al (data set I, this work)	40/47/13	~ 420	3.48
PZT/PVC	50/50/0	43.7	13.0
PZT/PVDF	50/50/0	68.1	14.0
PZT/PVDF/C	50.0/0.5/49.5	47.8	20.0
PZT/PVDF	50/50	56.0	14.0
PZT/PVDF	50/50	95.0	13.8
PZT/polyester	50/50	52	18
PZT/epoxy resin	63/37	15	25.3

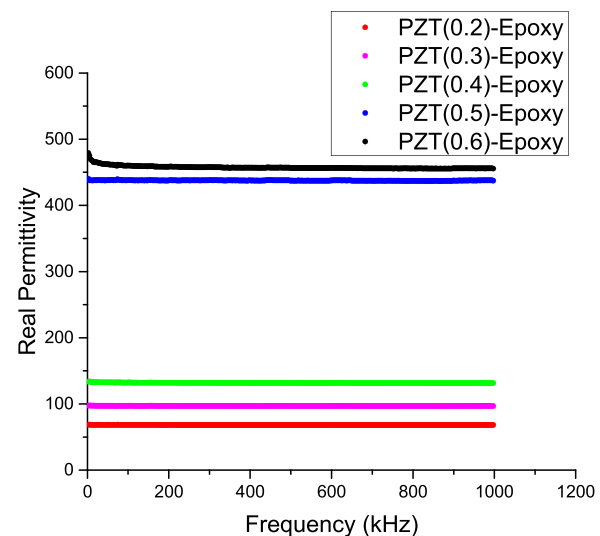


FIG. 8. (Color online) Real permittivity [dielectric constant, calculated from Eq. (1)] for data set G (PZT-epoxy) composite is plotted as a function of frequency. Data set G composites were corona poled at 15 kV/cm . As expected, the real permittivity is nearly constant over the frequency range and the maximum value occurs when the volume fraction of PZT is equal to 0.6.

spherical particles, where percolation occurs by way of particle contact. However, the percolation can also be achieved by way of electrical conduction through interparticle tunneling.³⁹ Electrical conduction that occurs via interparticle tunneling can diminish percolation threshold values in composites.

Another set of piezoelectric composite samples was fabricated to elucidate the limitations of the surface treatment process according to aluminum powder size. The additional samples were comprised of PZT, epoxy, and nanosized aluminum powder using the same process as described for data sample I. The nanosized aluminum powder was 99.95% purity with spherical morphology (APS: 18 nm) and purchased from MTI. The volume fraction of PZT was held constant at 0.40 while the volume fraction of the nanosize aluminum powder was varied from 0.01 to 0.17. These results are presented in Fig. 7. The maximum d_{33} value was measured to be 2.4 pC/N for 0.40 and 0.09 volume fractions of PZT and aluminum, respectively. This value is less than the maximum value reported for the samples fabricated using the micron-sized aluminum clusters (3.5 pC/N). This trend agrees with our previous work^{3,5} and the works of Refs. 40 and 41, where it was observed that use of the same process for the fabrication of nano- and micron-sized piezoelectric composites did not render the same piezoelectric strain values (when volume fractions of constituent materials were maintained). It is believed that this phenomenon is most likely due to the dominance of electrostatic forces between nanosized particles and greater resistivity of the nanocomposites in comparison to their counterparts, the microcomposites. Furthermore, the higher buildup of electrical charges on the surfaces of the nanosized particles leads to higher resistance at the interfaces between the nanoparticles and the other constituent phases within the composite, thereby resulting in diminished piezoelectric strain properties. Several researchers have concluded that as the size of powder particles are reduced, the influence of their surface properties plays a more dominant role in the ability of these materials to flow readily and ultimately mix within a matrix media. A higher degree of particle agglomeration was observed for the composites that incorporated nanosized aluminum inclusions.

The adhesion and cohesion, e.g., joining of surfaces of different and identical composition, respectively, was observed to be higher in the nanocomposites. The origin of this enhanced agglomeration was most likely due to the presence of electrostatically charged surfaces of the nanopowder.

The dielectric constants for the two-phase composite (PZT-epoxy, data set G) are plotted as a function of PZT volume fraction in Fig. 8. The dielectric constant for the two-phase composite does not appear to vary with frequency. The dielectric constant was found to increase with PZT content, where the average values were ~ 68.2 , ~ 96.9 , and ~ 131.7 for PZT volume fractions of 0.2, 0.3, and 0.4, respectively. These values were found to be higher than those of Refs. 18, 36, 42, and 43, which fabricated PZT-polymer 0–3 composites with PZT volume fractions of 50% (values in Table III).

The dielectric constants (real permittivity) for control 2 and data sets H and I are presented as a function of frequency for PZT and aluminum volume fractions of 0.2–0.4 and 0.01–0.17, in Figs. 9–11, respectively. The dielectric constants for all samples increase with the volume fraction of PZT and Al. The results indicate that all samples containing aluminum particles (corona and contact poled) had higher values of dielectric constant than the two-phase composites. The dielectric constant for control 2 was equal to ~ 156.7 for PZT and Al volume fractions equal to 0.2 and 0.13, respectively. This value is higher than composite samples that were comprised of 20% BaTiO₃ (80 nm particles) and 15% nickel²¹ whose dielectric constant was equal to ~ 100.8 . In general, the dielectric constant values of this work were found to be higher (in some cases a magnitude higher) than those in other works with similar volume fractions of PZT,⁴⁴ and others that included carbon black.⁴⁴ In Table III, the dielectric constant values are presented and compared.

The maximum dielectric constant values observed were for samples that were surface treated and corona polarized (data set I) when the volume fractions of PZT and aluminum were equal to 0.40 and 0.13, respectively. The influence of corona polarization on the dielectric constant is an issue of debate, where some scholars have found no difference in dielectric constants that were polarized using the parallel

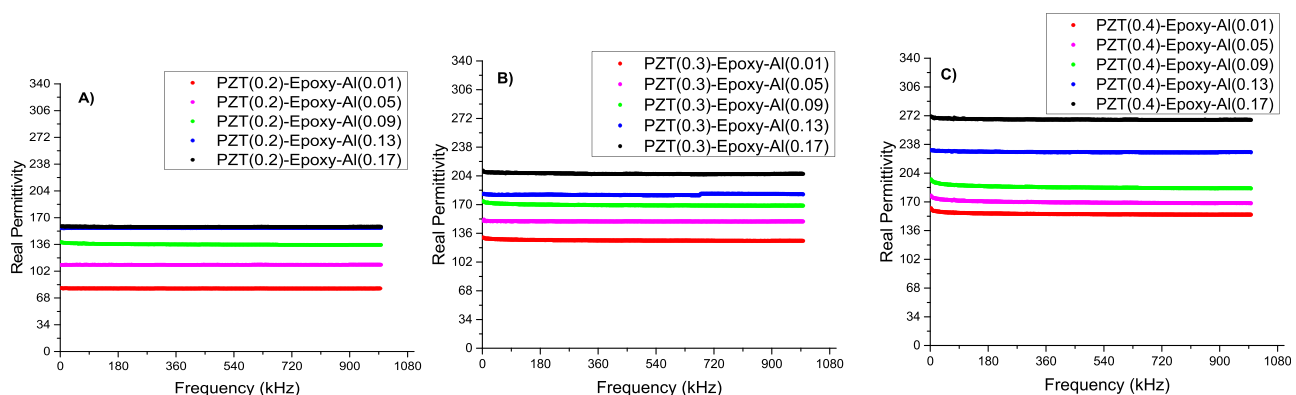


Fig. 9. (Color online) Real permittivity [dielectric constant, calculated from Eq. (1)] for control 2 (PZT-Epoxy-Al, contact poled at 12 kV/cm) is plotted as a function of frequency for (a) 0.2, (b) 0.3, and (c) 0.4 volume fraction of PZT. The maximum values of dielectric constant occur at 0.17 volume fraction of Al for 0.2, 0.3, and 0.4 volume fractions of PZT.

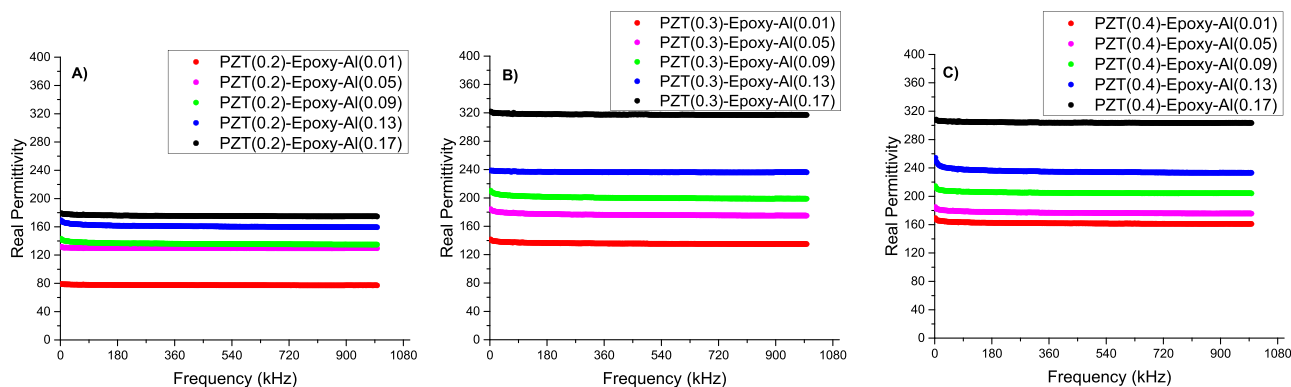


FIG. 10. (Color online) Real permittivity [dielectric constant, calculated from Eq. (1)] for data set H (PZT-epoxy-Al, nonsurface treated Al, corona poled at 15 kV/cm) is plotted as a function of frequency for (a) 0.2, (b) 0.3, and (c) 0.4 volume fractions of PZT. The maximum values of dielectric constant occur at 0.17 volume fraction of Al for 0.2, 0.3, and 0.4 volume fractions of PZT.

plate contact and corona polarization methods.³⁶ On the other hand, Waller *et al.*⁴⁹ found that polarization by the corona method produced higher dielectric constants than the conventional method. Based on the increases in dielectric constant and decrease in d_{33} at 0.13 volume fraction of PZT (in control 2 and data sets H and I), it is believed that the percolation threshold was achieved at the volume fraction of 0.13. The percolation threshold value is confirmed by the observation of resistivity plots of these composites as a function of frequency for PZT and aluminum volume fractions equal to 0.2–0.4 and 0.01–0.17, respectively, in Figs. 11–13. The dielectric characteristics of most materials are a function of ferroelectricity, charge density wave formation, hopping charge transport, the metal–insulator transition, and interface effects.⁵⁰ In Figs. 9–11 the dielectric constants increased as a function of aluminum volume fraction, which could be the result of hopping transport and interface effects. These mechanisms are validated by decreased resistivity in samples with aluminum content as demonstrated in Figs. 12–14.

The maximum value of dielectric constant was observed to be 411 for samples that were surface treated and corona polarized with volume fractions of PZT and aluminum that were equal to 0.40 and 0.13, respectively. The surface treated samples also displayed higher resistivity values, as can be seen in Fig. 14. Exposing the aluminum powder to

ethanol for 4 h resulted in surface morphology that was smoother and caused the deagglomeration of aluminum particle clusters, which may have contributed to better aluminum particle distribution within the composite (as shown in Fig. 4).

When the aluminum powder is exposed to ethanol for extended periods of time, self-passivation of the aluminum occurs, and an Al_2O_3 shell outside the metallic sphere is formed. This outer shell allows electrons in the metallic core to tunnel through it, which causes the composite to have a higher dielectric constant as observed in percolated systems. The Al_2O_3 shell around the Al particle also inhibits electron tunneling between successive Al particles, thereby leading to enhanced dielectric constants.^{27,51,52} Thinner Al_2O_3 layers on the aluminum particles leads to higher dielectric constants.⁵³ This interfacial polarization, the so-called Maxwell–Wagner, effect is responsible for the enhancement of dielectric constant.⁵⁴ The dielectric constants increase near the percolation threshold due to the presence of micro-capacitor networks, which can be represented as shown in Fig. 15. These networks are formed by neighboring conductive filler particles that sandwich PZT particles, which are insulated by the dielectric polymer matrix. Collectively, the networks contribute to the increase in capacitance^{55,56} of the samples. The formation of the network results in an increase

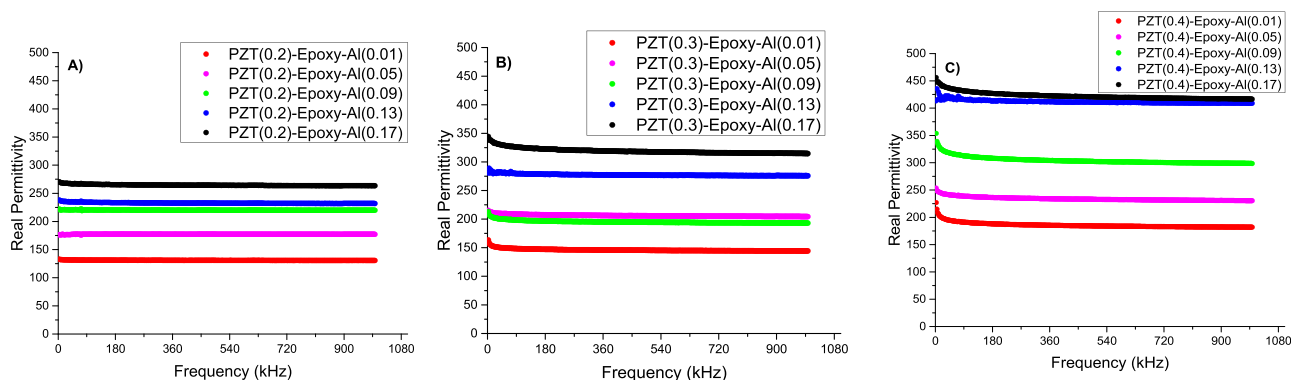


FIG. 11. (Color online) Real permittivity [dielectric constant, calculated from Eq. (1)] for data set I (PZT-epoxy-Al, surface treated Al, corona poled at 15 kV/cm) is plotted as a function of frequency for (a) 0.2, (b) 0.3, and (c) 0.4 volume fractions of PZT. The maximum values of dielectric constant occur at 0.17 volume fraction of Al for 0.2, 0.3, and 0.4 volume fractions of PZT.

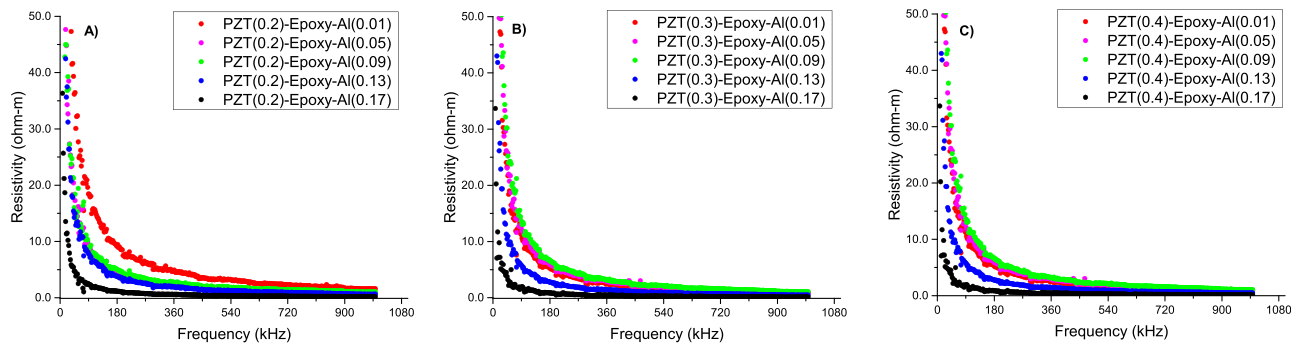


FIG. 12. (Color online) Resistivity for control 2 (PZT-epoxy-Al, contact poled at 12 kV/cm) is plotted as a function of frequency for (a) 0.2, (b) 0.3, and (c) 0.4 volume fraction of PZT. The minimum values of resistivity occur for 0.17 volume fraction of Al for 0.2, 0.3, and 0.4 volume fractions of PZT.

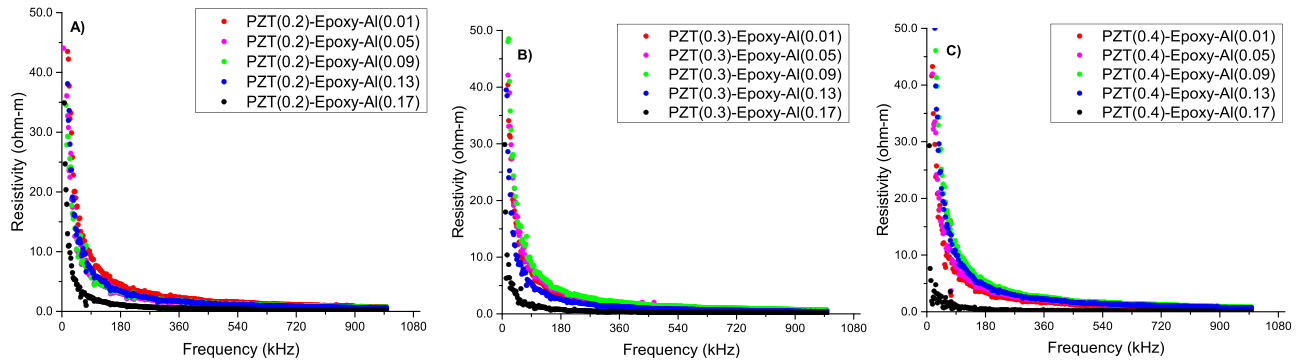


FIG. 13. (Color online) Resistivity for data set H (PZT-epoxy-Al, nonsurface treated Al, corona poled at 15 kV/cm) is plotted as a function of frequency for (a) 0.2, (b) 0.3, and (c) 0.4 volume fractions of PZT. The minimum value of resistivity occurs for 0.17 volume fraction of aluminum for 0.2, 0.3, and 0.4 volume fractions of PZT.

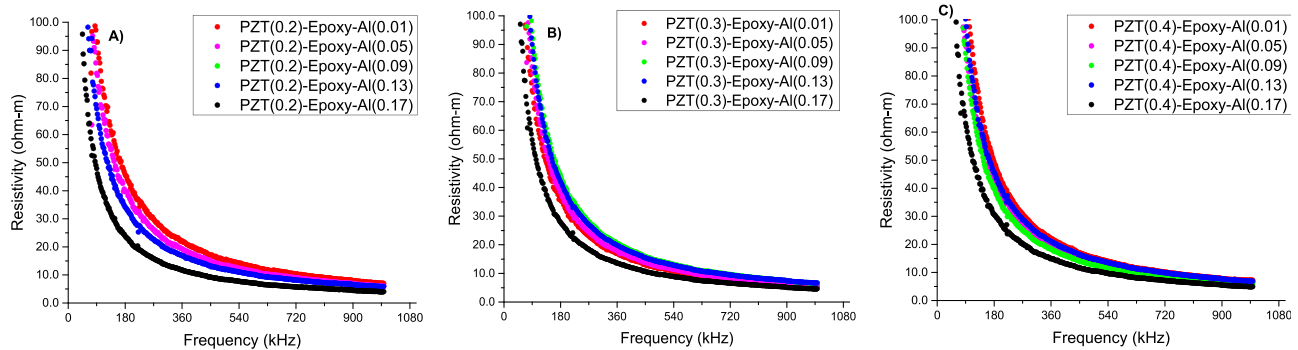


FIG. 14. (Color online) Data set I (PZT-epoxy-Al, surface treated Al, corona poled at 15 kV/cm) is plotted as a function of frequency for (a) 0.2, (b) 0.3, and (c) 0.4 volume fractions of PZT. The minimum value for resistivity occurs for 0.17 volume fraction of aluminum for 0.2, 0.3, and 0.4 volume fractions of PZT.

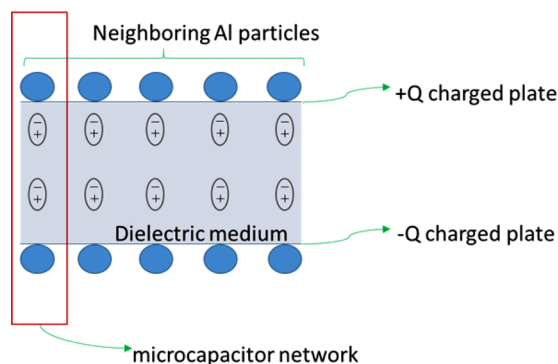


FIG. 15. (Color online) Microcapacitor network.

in the local electric field when the conductive fillers are close together, which promotes migration and accumulation of charge carriers at the interfaces between the aluminum particles and the polymer matrix.⁵⁴ The charges generated are accumulated at the interfaces as a result of Coulomb blockade by the insulating matrix until the conductive fillers approach each other, and the charges are relaxed by tunneling or by ohmic conduction.

IV. SUMMARY AND CONCLUSIONS

Three phase piezoelectric PZT-Al-epoxy composites have been fabricated and polarization using corona and contact methods. The volume fractions of PZT and aluminum were

varied from 0.2 to 0.4 and 0.0 to 0.17, respectively. The piezoelectric strain coefficient and dielectric constant increased with PZT and Al volume content. However, the percolation threshold is believed to have been achieved for a volume fraction of 0.13 of aluminum, which was validated by observation of the resistivity of samples as a function of frequency and volume fraction. The resistivity of the samples decreased as a function of PZT and aluminum, where sharp decreases in resistivity were observed for the volume fraction above 0.13 of aluminum.

ACKNOWLEDGMENTS

This material is based upon work supported by the National Science Foundation under Grant Award Nos.: EEC-1263250, EEC-1009797 and DGE-0903661. In addition, the authors would like to recognize support from the New Jersey Space Grant Consortium and the Rutgers Research in Science and Engineering (RiSE) program.

- ¹M. A. Rahman, B. C. Lee, D. T. Phan, and G. S. Chung, *Smart Mater. Struct.* **22**, 085017 (2013).
- ²I. Babu, D. A. van den Ende, and G. de With, *J. Phys. D: Appl. Phys.* **43**, 425402 (2010).
- ³S. Banerjee and K. A. Cook-Chennault, *J. Eng. Mater. Technol.* **133**, 041016 (2011).
- ⁴S. Banerjee and K. A. Cook-Chennault, *J. Eng. Mater. Technol.* **133**, 041005 (2011).
- ⁵S. Banerjee and K. A. Cook-Chennault, *Composites, Part A* **43**, 1612 (2012).
- ⁶S. Banerjee and K. A. Cook-Chennault, *Adv. Cem. Res.* **26**, 63 (2014).
- ⁷S. Banerjee, W. Du, L. Wang, and K. A. Cook-Chennault, *J. Electroceram.* **31**, 148 (2013).
- ⁸K. A. Cook-Chennault, N. Thambi, M. A. A., and E. B. Hameyie, *Bull. Sci. Technol. Soc.* **28**, 496 (2008).
- ⁹K. A. Cook-Chennault, N. Thambi, and A. M. Sastry, *Smart Mater. Struct.* **17** (2008).
- ¹⁰G. H. Feng, *Smart Mater. Struct.* **16**, 2636 (2007).
- ¹¹M. G. Smith, L. C. Chow, and N. Molin, presented at the 12th AIAA/CEAS Aeroacoustics Conference, Cambridge, MA, 2006 (unpublished).
- ¹²R. Y. Ting, *IEEE Trans. Instrum. Meas.* **41**, 64 (1992).
- ¹³R. Y. Ting, *Appl. Acoust.* **41**, 325 (1994).
- ¹⁴H. Banno and K. Ogura, *Jpn. J. Appl. Phys., Part 1* **30**, 2247 (1991).
- ¹⁵H. Banno and K. Ogura, *Jpn. J. Appl. Phys., Part 1* **30**, 2250 (1991).
- ¹⁶J. A. Hossack and R. L. Bedi, *Ferroelectr. Polym. Ceram. Polym. Compos.* **92–9**, 301 (1994).
- ¹⁷Y. M. Poon, C. H. Ho, Y. W. Wong, and F. G. Shin, *J. Mater. Sci.* **42**, 6011 (2007).
- ¹⁸K. Arlt and M. Wegener, *IEEE Trans. Dielectr. Electr. Insul.* **17**, 1178 (2010).
- ¹⁹A. Safari, *J. Phys. III France* **4**, 1129 (1994).
- ²⁰B. S. Prakash and K. B. R. Varma, *Compos. Sci. Technol.* **67**, 2363 (2007).
- ²¹H. W. Choi, Y. W. Heo, J. H. Lee, J. J. Kim, H. Y. Lee, E. T. Park, and Y. K. Chung, *Integr. Ferroelectr.* **87**, 85 (2007).
- ²²J. M. Park, H. Y. Lee, J. J. Kim, E. T. Park, and Y. K. Chung, *IEEE Trans. Ultrason. Ferroelectr. Freq. Control* **55**, 1038 (2008).
- ²³C. Zhang, J. F. Sheng, C. A. Ma, and M. Sumita, *Mater. Lett.* **59**, 3648 (2005).
- ²⁴X. B. Ding and X. Yan, *J. Appl. Polym. Sci.* **102**, 3181 (2006).
- ²⁵W. Zheng and S. C. Wong, *Compos. Sci. Technol.* **63**, 225 (2003).
- ²⁶S. Banerjee, R. Kappera, K. A. Cook-Chennault, and M. Chhowalla, *Energy Environ. Focus* **2**, 195 (2013).
- ²⁷X. W. Xu and C. P. Wong, in *54th Electronic Components & Technology Conference* (2004), Vols 1 and 2, pp. 496–506.
- ²⁸APC International, Ltd., *Physical and Piezoelectric Properties of APC Materials* (APC International, PA, 2013).
- ²⁹J. Manassen, *Adv. Catal.* **16**, 49 (1966), <http://www.sciencedirect.com/science/article/pii/S036005640860351X>.
- ³⁰H. Adkins and P. P. Perkins, *J. Am. Chem. Soc.* **47**, 1163 (1925).
- ³¹H. N. Chiang, S. Nachimuthu, Y. C. Cheng, N. P. Damayanti, and J. C. Jiang, *Appl. Surf. Sci.* **363**, 636 (2016).
- ³²W. Nhuapeng and T. Tunkasiri, *J. Am. Ceram. Soc.* **85**, 700 (2002).
- ³³K. H. Han, A. Safari, and R. E. Riman, *J. Am. Ceram. Soc.* **74**, 1699 (1991).
- ³⁴K. H. Lam and H. L. W. Chan, *Compos. Sci. Technol.* **65**, 1107 (2005).
- ³⁵J. Liu, D. Tang, and J. Li, *Rare Met. Mater. Eng.* **36**, 411 (2007), available at http://en.cnki.com.cn/Article_en/CJFDTOTAL-COSE2007S1120.htm.
- ³⁶G. Rujijanagul, S. Boonyakul, and T. Tunkasiri, *J. Mater. Sci. Lett.* **20**, 1943 (2001).
- ³⁷G. Rujijanagul, S. Jompruan, and A. Chaipanich, *Curr. Appl. Phys.* **8**, 359 (2008).
- ³⁸H. Scher and R. Zallen, *J. Chem. Phys.* **53**, 3759 (1970).
- ³⁹X. Jing, W. Zhao, and L. Lan, *J. Mater. Sci. Lett.* **19**, 377 (2000).
- ⁴⁰H. H. Lee, K. S. Chou, and Z. W. Shih, *Int. J. Adhes. Adhes.* **25**, 437 (2005).
- ⁴¹W. Jia, R. Tchoudakov, R. Joseph, M. Narkis, and A. Siegmans, *J. Appl. Polym. Sci.* **85**, 1706 (2002).
- ⁴²B. Satish, K. Sridevi, and M. S. Vijaya, *J. Phys. D: Appl. Phys.* **35**, 2048 (2002).
- ⁴³Q. M. Liu, J. C. Tu, X. Wang, W. X. Yu, W. T. Zheng, and Z. D. Zhao, *Carbon* **50**, 339 (2012).
- ⁴⁴X. F. Liu, C. X. Xiong, H. J. Sun, L. J. Dong, R. Li, and Y. Liu, *J. Wuhan Univ. Technol.* **20**, 60 (2005).
- ⁴⁵X. F. Liu, C. X. Xiong, H. J. Sun, L. J. Dong, R. Li, and Y. Liu, *Mater. Sci. Eng. B* **127**, 261 (2006).
- ⁴⁶S.-B. B. T.-X. Xu, J.-C. Han, and D. Shan-yi, *Acta Mater. Compositae Sinica* **17**, 1 (2000).
- ⁴⁷E. Venkatragavaraj, B. Satish, P. R. Vinod, and M. S. Vijaya, *J. Appl. Phys. D: Appl. Phys.* **34**, 487 (2001).
- ⁴⁸W. Thamjaree, W. Nhuapeng, A. Chaipanich, and T. Tunkasiri, *Appl. Phys. A* **81**, 1419 (2005).
- ⁴⁹D. Waller, T. Iqbal, and A. Safari, *J. Am. Ceram. Soc.* **72**, 322 (1989).
- ⁵⁰P. Lunkenheimer, S. Krohns, S. Riegg, S. G. Ebbinghaus, A. Reller, and A. Loidl, *Eur. Phys. J.-Spec. Top.* **180**, 61 (2010).
- ⁵¹T. Lewis, *J. Phys. D: Appl. Phys.* **38**, 202 (2005).
- ⁵²C. Yang, H. S. Song, and D. B. Liu, in *Advanced Materials*, edited by Z. Cao, Z. Q. Cao, L. Sun, and Y. H. He (2011), Vol. 239–242, Parts 1–4, pp. 3113–3118.
- ⁵³J. Xu and C. Wong, *Appl. Phys. Lett.* **87**, 082907 (2005).
- ⁵⁴C.-W. Nan, Y. Shen, and J. Ma, in *Annual Review of Materials Research*, edited by D. R. Clarke, M. Rühle, and F. Zok (2010), Vol. 40, pp. 131–151.
- ⁵⁵D. J. Bergman and Y. Imry, *Phys. Rev. Lett.* **39**, 1222 (1977).
- ⁵⁶C. Pecharrmán and J. S. Moya, *Adv. Mater.* **12**, 294 (2000).